

Chapter 2

Modeling the SOA'S MCW and IR Radiation Characteristics and Their Relationship with Surface Heat Fluxes at Synoptic Time Scales

2.1 Modeling the SOA's Brightness Temperature with ATLANTEX-90 Vessel Experiment Data

2.1.1 Description of the Initial Data

This study used the results of the ATLANTEX-90 experiment obtained from the R/Vs *Victor Bugaev*, *Musson*, and *Volna*, which completed the final phase of the “RAZREZY” scientific project on large-scale ocean–atmosphere heat and dynamic interactions in the North Atlantic energy active zones. From this experiment, we extracted data that were obtained during the so-called stationary phase (April 4–21, 1990), which had the following features:

- (a) Maximum regularity of the meteorological and, especially, aerologic measurements during this period
- (b) Possibility of a fine analysis of the temporal dynamics of the oceanic and atmospheric parameters due to the fixed (stationary) positions of the R/Vs *Victor Bugaev*, *Musson*, and *Volna*

The research vessels were situated in three areas of the Gulf Stream delta: a southern periphery of the basic Gulf Stream water flow (R/V *Victor Bugaev*), its southern stream (R/V *Musson*), and an eastern branch of the Labrador Current (R/V *Volna*). This zone is characterized by strong synoptic variability in oceanic and atmospheric parameters, which is caused by an influence of the subpolar hydrological front (SHF) as a result of the interaction between the cold Labrador Current and the warm quasi-stationary anticyclon rings of the Gulf Stream. An important attribute of this zone is the intensive horizontal circulation of the atmosphere: For approximately 50 % of the time, this area of the North Atlantic feels the influence of powerful midlatitude cyclones, which excite intensive variations of the atmospheric temperature and humidity as well as boundary heat fluxes (Lappo et al. 1990).

The following parameters in each vessel experiment were selected for further analysis:

- (1) Hourly values of the ocean surface temperature t_s , near-surface air temperature t_a and humidity (vapor pressure) e , and wind speed V derived from hydrological and meteorological measurements (more than 1000 measurements with 1-h resolution)
- (2) Results of aerologic measurements of the total atmospheric water vapor content Q within 10–16,000 m at 20 levels with periodicity 6 h (more than 200 aerologic measurements)
- (3) Hourly estimates of turbulent heat fluxes q_h and vapor q_e parameterized from hourly measurements of the parameters t_s , t_a , V and e

A fragment of the stationary phase of the ATLANTEX-90 experiment (from April 8–13, 1990) was analyzed in detail. In this period, all vessel oceanographic and meteorological sensors responded synchronously to a powerful cyclone in this area of the North Atlantic.

2.1.2 Model of the SOA's Natural Radiation with Microwaves and Infrareads

Satellite measurements of the intensity of natural MCW radiation (at millimeters and centimeters) are the result of a composition of oceanic and atmospheric vertical electromagnetic fluxes and their couplings. Therefore, we ought to consider these mediums together as the ocean–atmosphere system (SOA).

To calculate the SOA's natural radiation intensity for microwaves and infrareads using vessel measurement data, a model is required to assimilate oceanographic and meteorological parameters, as well as data on the vertical distribution of the air temperature, humidity, and pressure obtained from aerologic measurements.

Here, we use the plane-layer model of natural radiation (Basharinov et al. 1974). This model uses observations from altitude H for the intensity of radiation of the SOA I , which is the sum of three components:

$$I = I_1 + I_2 + I_3 \quad (2.1)$$

where

$$I_1 = I_s \exp(-\tau) \quad (2.2)$$

which is the intensity of upward radiation flux from the water (oceanic) surface I_s attenuated in the atmosphere. The quantity I_s is proportional to the emissivity of the water surface and its thermodynamic temperature T_s ($T_s = t_s + 273$).

$$I_2 = \int_0^H I_a(h) \exp[\tau(h) - \tau(H)] dh \quad (2.3)$$

which is the intensity of the upward atmosphere radiation flux. This is computed by summing the partial fluxes $I_a(h)$, taking into account the proper attenuation values of the atmosphere layers.

$$I_3 = \exp[-\tau(H)] R \int_0^H I_a(h) \exp[-\tau(h)] dh \quad (2.4)$$

which is the intensity of the atmosphere's downward radiation flux reflected by the water surface.

$$\tau(h) = \int_0^h \gamma(h') dh' \quad (2.5)$$

is the integral attenuation of the radiation by the atmosphere, which depends on the linear absorption factor γ and the thickness h of the absorbing layer measured from the ocean surface ($h = 0$); R is the coefficient of reflection of the atmosphere's downward radiation flux from the water surface.

The intensity of natural MCW and IR radiation I_s of the water surface is proportional to the following:

At microwaves	At infrareds
$I_s = \epsilon T_s$;	$I_s = B(T_s)$,

where $I_s(h)$ is the intensity of the water surface's upward radiation; ϵ is the water surface emissivity at microwaves; and $B(T_s)$ is the Plank function with the argument T_s .

The intensity of the atmosphere's MCW and IR natural radiation I at level h is determined as follows:

At microwaves	At infrareds
$I_a(h) = T_a(h) \gamma(h)$;	$I_a(h) = B[T_a(h)] \gamma(h)$,

where $T_a(h)$ is the thermodynamic temperature of the atmosphere at the level h in Kelvins ($T_a(h) = t_a(h) + 273$). $B[T_a(h)]$ is the Plank function with the argument $T_a(h)$.

In the MCW range of wavelengths, where the Rayleigh–Jeans approximation is valid, respective values of the brightness temperature are used as a measure of the radiation intensity of different components of the SOA. To characterize the IR radiation intensity I , we use the concept of effective (radiation) temperature T^r , defining it from the equation $B(T^r)$ —that is, as a thermodynamic temperature of the absolute (ideal) black body with a radiation intensity equal to I .

2.2 SOA Brightness Temperature Contrasts and Their Comparison with Heat Fluxes

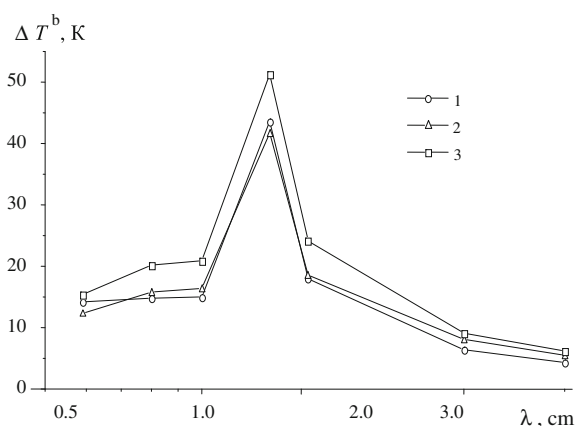
2.2.1 Calculations of SOA Brightness Temperature at Microwaves

Here, we use the model (2.1)–(2.5) to analyze daily and synoptic variations of SOA brightness temperatures in the wavelength range of 0.5–5.0 cm for the stationary phases of the ATLANTEX-90 experiment in the areas of the *Victor Bugaev*, *Musson*, and *Volna* vessels. The water surface's brightness temperature T^b was calculated according to the principles stated in Basharinov et al. (1974). The numerical estimates of the linear absorption factor γ were obtained by taking into account the dominating role of the atmosphere's water vapor and molecular oxygen using the theoretical relations of the absorption factor γ with the air temperature, humidity, and pressure; the computations of the SOA's brightness temperature were made for the case of a cloudless atmosphere.

The response of the SOA's natural MCW radiation to the variability of heat fluxes at the ocean–atmosphere interface was the most distinct during April 8–13, 1990, when a powerful cyclone occurred. Over this period, variations of the total (sensible + latent) heat fluxes were more than 800 W m^{-2} for the *Victor Bugaev*, 500 W m^{-2} for the *Musson*, and about 400 W m^{-2} for the *Volna* (Gulev et al. 1994). Among the spectral ranges used to calculate the SOA brightness temperature (5.4, 5.6, 5.9 mm, 0.8, 1.0, 1.35, 1.6, 3.2, and 5.0 cm), the brightness temperature contrasts over this time interval were greatest in the wavelength range of 0.59–1.6 cm, which corresponds to the resonant effect of the atmospheric oxygen and water vapor on the upward radiation (Fig. 2.1).

The attenuation band of natural radiation in atmospheric water vapor at a wavelength of 1.35 cm and its vicinities plays a special role in an analysis of the ocean–atmosphere heat interaction; this region of the MCW spectrum will be the focus of our interests when studying the heat processes at the ocean–atmosphere boundary.

Fig. 2.1 Spectral dependence of the SOA's brightness temperature contrast ΔT^b in the wavelength range of 5 mm–5 cm during the passage of a cyclone (April 8–13) through the location of the RV/s *V. Bugaev* (1), *Musson* (2) and *Volna* (3)



2.2.2 Relationship Between the SOA's Brightness Temperature and Heat Fluxes

The contributions of different layers to the radiation properties of the SOA and the effect on their relationship with the surface heat fluxes on the synoptic time scale were evaluated using the model (2.1)–(2.5) for various cases. In the first case, the downward-facing sensors (radiometers) were placed in free air to simulate satellite observations. In the second case, which simulates measurements aboard an aircraft, the downward sensors were placed at the boundary between free air and the atmospheric boundary layer. In the third case, the upward and downward sensors were placed 10–20 m above the water surface to simulate measurements aboard the vessels (this scheme is described in detail in Chap. 4).

A close correlation was observed between the estimated variations of the SOA brightness temperature and near-surface total heat fluxes at the *satellite*, *aircraft*, and *vessel* levels. This idea is illustrated in Figs. 2.2 and 2.3, which compare the values of $T_{1.35}^b$ (the brightness temperature at a wavelength of 1.35 cm) and $T_{0.59}^b$ (the brightness temperature at a wavelength of 5.9 mm), with total heat fluxes q_{he} obtained aboard the *V. Bugaev*, *Musson*, and *Volna*.

The satellite level of observations corresponds to the upper boundary of the troposphere. The aircraft level corresponds to the upper boundary of the atmosphere's boundary layer, whereas the vessel level corresponds to the upper boundary of the near-surface atmospheric layer.

It can be seen from the Figs. 2.2 and 2.3 that, in response to the increase in the fluxes q_{he} , the SOA's natural MCW radiation diminishes its brightness temperature T^b and vice versa: as the value of q_{he} decreases, T^b grows. Over this period, the brightness temperature variations are, on average, 15–20 K at the wavelength 5.9 mm and 30–40 K at 1.35 cm. In addition, the response of the brightness temperature lags behind the heat flux variation by 6–12 h.

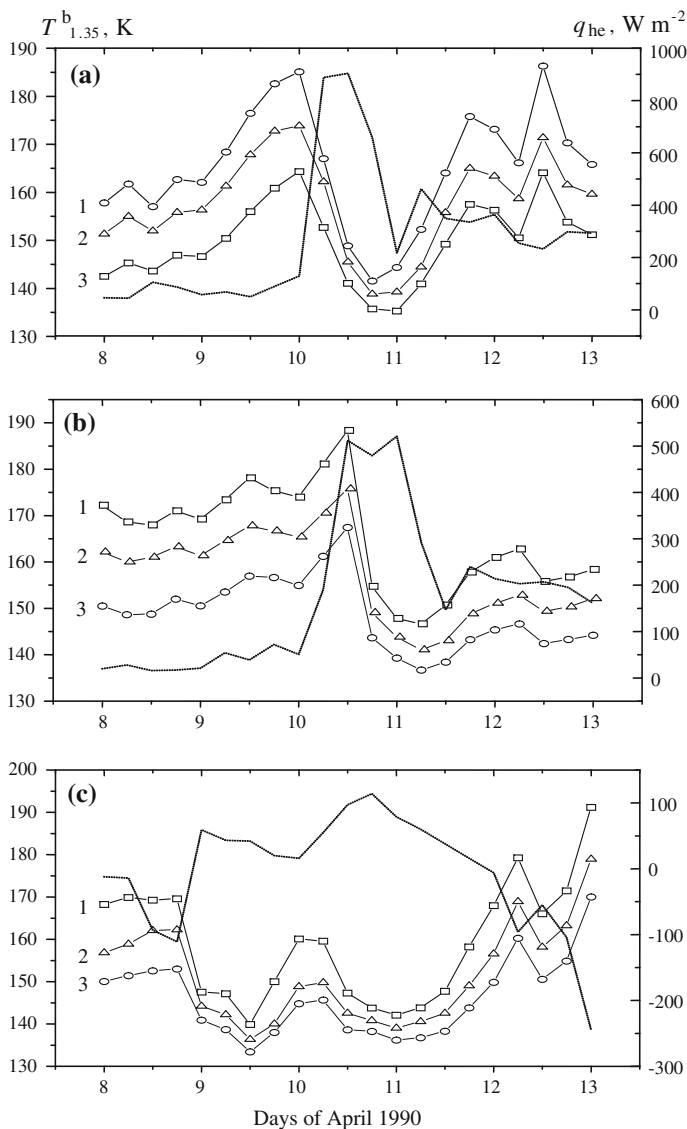


Fig. 2.2 Comparison of q_{he} (dotted line) with the estimates $T^b_{1.35}$ for the locations of the *V. Bugaev* (a), *Musson* (b) and *Volna* (c) during April 8–13, 1990 (ATLANTEX-90 experiment). Simulation of satellite (1), aircraft (2) and vessel (3) observations

The response of brightness temperature to surface heat fluxes depends only slightly on whether the measurements were carried out in the atmospheric surface layer, the top of the atmospheric boundary layer, or the free atmosphere. In these cases, the brightness temperature differs in magnitude but satisfies the following condition: the higher the observation height, the greater the parameter T^b .

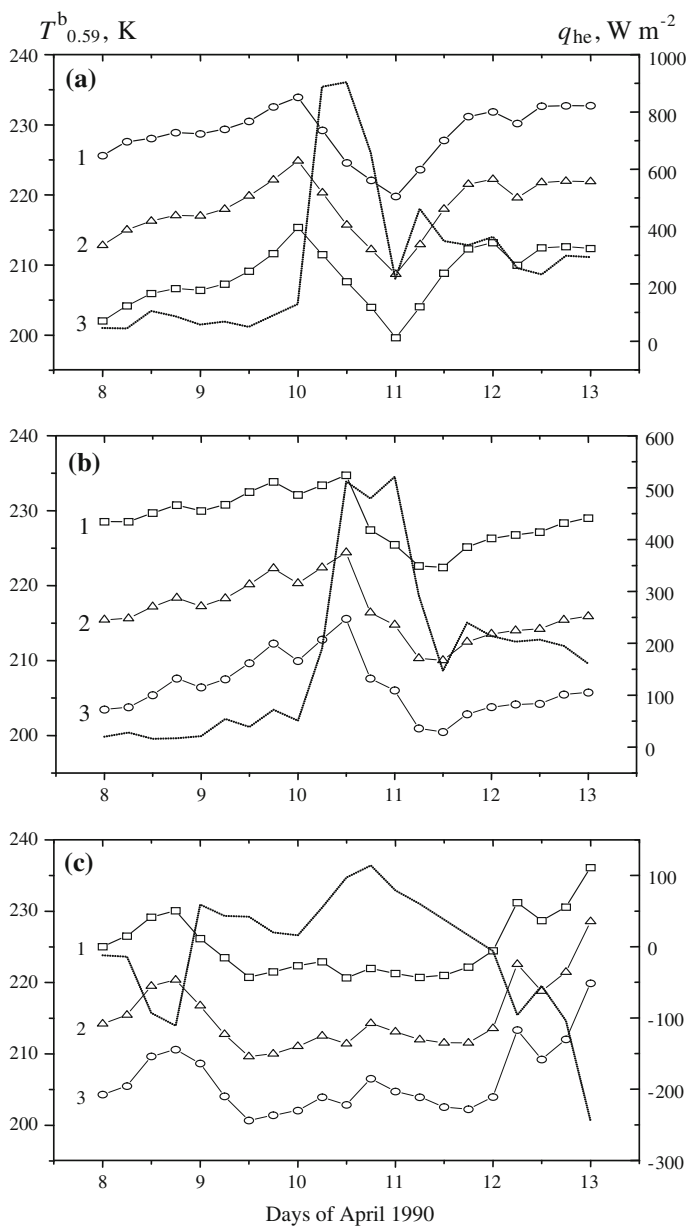
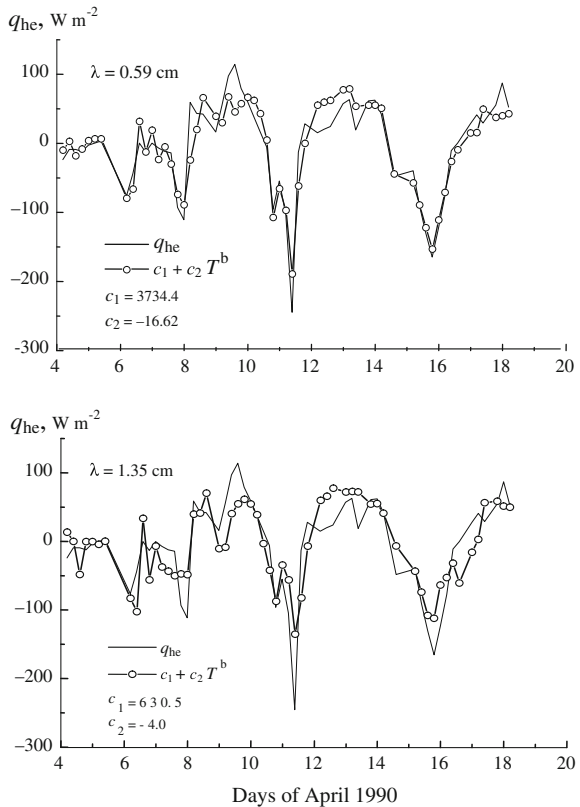


Fig. 2.3 The same data as in Fig. 2.2, but for the wavelength of 5.9 mm

We studied linear regressions between 6-h samples of the total heat flux q_{he} at the ocean–atmosphere interface recorded by the R/V *Volna* in the experiment ATLANTEX-90, as well as the SOA brightness temperatures at the wavelengths of 5.9 mm and 1.35 cm computed for the satellite-level case from the meteorological and aerologic measurements aboard this vessel in the form $q_{\text{he}} = c_1 + c_2 T^b$ (Fig. 2.4). An intimate relationship is shown between the synoptic variations of heat fluxes and model estimates of the SOA brightness temperature. For 6-h samples of the parameters q_{he} and T^b in the resonance bands of molecular oxygen and atmospheric water vapor, the least absolute error of approximating the total heat flux q_{he} by the brightness temperature T^b is 26–28 W m^{-2} for a flux variation amplitude of 320 W m^{-2} .

The relative variations of the regression coefficients c_1 and c_2 are 13–15 %, with the regression coefficient c_2 being negative in both cases. This means that the heat flux and the brightness temperature vary in antiphase: an increase in the parameter q_{he} causes T^b to decrease and vice versa. It is remarkable that the intensity variations of the SOA's natural MCW radiation correlates well with variations of the heat fluxes in this case, although the accuracy of finding the brightness temperature, and

Fig. 2.4 Six-hour samples of total heat fluxes q_{he} , as the linear combinations of SOA brightness temperatures at the wavelengths 0.59 cm and 1.35 cm. Stationary phase of the experiment ATLANTEX-90 (R/V *Volna*)

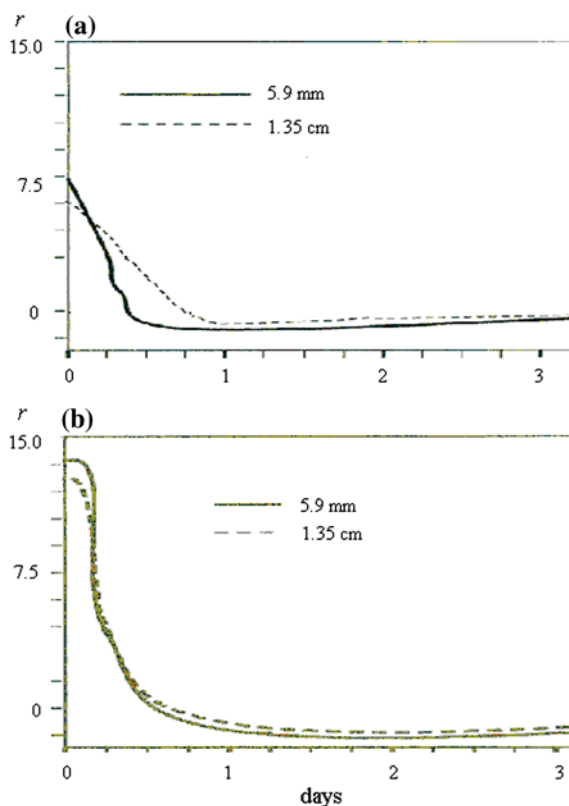


especially the heat fluxes, is not very high. The relative error involved in the model brightness temperature values found under the hydrometeorological conditions of the ATLANTEX-90 experiment is estimated to be 5–10 %, while that of the heat fluxes determined by the bulk parameterizations given in Chap. 1 may be as great as several tens of percent (Gulev et al. 1994). This factor substantiates the idea of using passive MCW radiometric data as *natural* characteristics of the ocean–atmosphere heat interaction.

2.2.3 Computation of the Brightness Temperature Response to the Heat Fluxes Variations

We analyzed Grankov et al. (2010) more rigorously with regard to the phenomenon of a time delay of the SOA brightness temperature response in the resonant spectral domains of 0.59 cm and 1.35 cm, compared with the variations of surface heat fluxes resting upon the results adjusted above (Fig. 2.5).

Fig. 2.5 Sensitivity of the SOA brightness temperature at the wavelengths of 0.59 and 1.35 cm to heat flux variations in areas observed by the R/Vs *V. Bugaev* (a) and *Volna* (b)



Duamel's integral equation let us calculate the function $r(t)$ of the brightness temperature T^b response (sensitivity) to the total heat flux q_{he} variations:

$$T^b(t) = \cdot \int_0^t q(\tau) \cdot r(t - \tau) \cdot d\tau \quad (2.6)$$

Formula (2.6) can be considered as a modification of the classic Volterra's equations of the first kind inherent to the class of equations of the convolution type. We proposed an iterative procedure to determine the function $r(t)$ as a linear superposition of the exponential functions:

$$r(t) = \sum_{i=1}^N a_i \exp(-b_i t) \quad (2.7)$$

where coefficients a_i and b_i are calculated from the condition of minimal discrepancy between the SOA brightness temperature values and their approximations, characterized by values of the root-mean square (rms) error. The calculations show that the value $N = 6$ in Formula (2.7) is acceptable for this task; a mean value of the rms error in this case does not exceed 5–7 %.

The results shown in Fig. 2.5b for the vessel *Volna* are especially useful for the fuzziness of variations of the parameters T^b and q_{he} (see Figs. 2.2c and 2.3c). This case is distinguished from the cases illustrated in Figs. 2.2a, b and 2.3a, b, where the time shift between these parameters is noticeably obvious without any mathematical analysis.

Table 2.1 illustrates the results of an analysis of the role of a time delay of the SOA response on the synoptic surface heat fluxes. Here, we present the data from a regression analysis [the coefficient of correlation R and discrepancy d (rms)] between simulated estimates of the SOA brightness temperatures at the wavelengths of 0.59 and 1.35 cm and the heat flux data collected from the vessel *Musson* during the stationary phase of the ATLANTEX-90 experiment. It follows from Table 2.1 that maximal values of the coefficient of correlation ($R = 0.84$ – 0.86) and minimal values of the discrepancy ($d = 85$ – 93) take place when Δt is 12 h.

Table 2.1 Influence of the time shift Δt between the time samples of the SOA brightness temperature at the wavelengths 0.59 cm (1) and 1.35 cm (2) and heat fluxes on their correlation R and rms d (R/V *Musson*)

Time shift Δt	0 h	6 h	12 h	18 h
Correlation R (1)	0.25	0.67	0.86	0.84
Correlation R (2)	0.34	0.74	0.85	0.71
Discrepancy d , $W\ m^{-2}$ (1)	160	124	85	98.7
Discrepancy d , $W\ m^{-2}$ (2)	157	113	93	127.3

The peak of heat flux variations is $900\ W\ m^{-2}$

Thus, while carrying out a comparison of these data, we have to take into account the factor of a time shift between the surface heat fluxes and the brightness temperature variations in the synoptic range of time scales.

2.3 Analysis of the Factors Forming the Relationship Between Natural MCW Radiation and Heat Characteristics of the SOA

2.3.1 *Parameters and Mechanisms that Form Relationships Between the Brightness Temperature and Surface Heat Fluxes*

A problem that has been repeatedly discussed by teams at the Institute of Radioengineering and Electronics, the Institute of Space Research; and the Institute of Oceanology, Russian Academy of Sciences is how the SOA brightness temperature (simulated or satellite measured), for which an effectively radiating 2- to 5-km-thick stratum is responsible, can be related to the temperature and humidity properties of a much thinner (roughly 10-m-thick) near-water atmospheric layer.

Here, we examine the importance (priority) of ocean surface parameters and some parameters of different atmospheric layers—that is, their effect on the correlation between heat and humidity exchange characteristics and the MCW radiation of the SOA on the *synoptic* time scales. To this end, a regression analysis of relationships between variations of simulated brightness temperatures ΔT^b and total heat fluxes Δq_{he} was made based on the data accumulated from the R/V *Volna* in the ATLANTEX-90 experiment stationary phase with the following formulas:

$$\Delta q_{\text{he}} = k_1 \Delta T_{i1} + k_2 \Delta T_{i2}; \quad i = 1, \dots, 4, \quad (2.8)$$

Here, the indices 1 and 2 are attached to the SOA brightness temperature of natural radiation in certain pieces of the MCW spectrum characterized by the wavelengths λ_1 and λ_2 . Due to the index i , we can divide the influence of parameters forming the ocean–atmosphere heat interaction, such as the ocean surface temperature t_s ($i = 1$), the near-surface wind speed V ($i = 2$) and temperature t_a ($i = 3$), as well as the total water vapor content Q ($i = 4$). ΔT_{i1} and ΔT_{i2} are the brightness temperature variations at these wavelengths caused by variations of these parameters.

Then, we used an ordered elimination method to reveal the contribution of one or another parameter simultaneously to the heat exchange process and the SOA natural radiation in different parts of the MCW range of wavelengths. Table 2.2 lists the errors due to the approximation of the total heat fluxes q_{he} by the brightness temperatures of the SOA radiation in the wavelength range of 0.56–3.2 cm.

Table 2.2 Root-mean-square errors of approximation of the total heat fluxes by the SOA brightness temperatures simulated with various radiation models (the generalized model is shown in column *d*, with the simplified model shown in the other columns)

Wavelength, cm	Approximation error, W m ⁻²				
	<i>d</i>	<i>d</i> _{<i>t</i>_s}	<i>d</i> _{<i>V</i>}	<i>d</i> _{<i>t</i>_a}	<i>d</i> _{<i>Q</i>}
0.56	27.8	27.8	28.2	48.5	27.8
0.8	26.6	26.8	27.3	27.0	37.8
1.35	27.0	27.2	28.4	27.5	35.9
1.6	26.1	26.3	27.8	26.5	35.9
3.2	34.2	34.2	30.2	34.3	39.4

In Table 2.2, column *d* shows the discrepancy (rms) between the parameter q_{he} and the linear combinations of the parameters ΔT_{i1} and ΔT_{i2} , whose values were computed by a least-squares method taking into account variations of all basic parameters of the SOA (t_s , t_a , V , and Q). In columns d_{t_s} , d_V , d_{t_a} , and d_Q , the effects of the ocean surface temperature t_s , the near-surface wind speed V and temperature t_a , and the total water vapor content Q , respectively, are excluded (neutralized). The table shows that the influence of the ocean surface temperature is easier compared with the atmospheric parameters t_a and Q . This is a consequence of heat inertia in the ocean upper layer: it is seen from the ATLANTEX-90 experimental data that synoptic variations of the OST are less by an order of the temperature and humidity variations in the near-surface atmosphere.

We also analyzed the relationship between synoptic variations of the parameter q_{he} and variations of the SOA brightness temperature derived as a result of the imitation of satellite and aircraft measurements with the downward MCW sensors, as well as ship measurements with upward (1) and downward (2) sensors (antennas): these results are presented in Table 2.3. Computations of the SOA brightness temperatures were performed using the radiation model (2.1)–(2.5) for the six-hourly samples taken from measurements of the parameters t_s , V , t_a , and Q observed aboard the vessel *Volna* at the stationary phase of the ATLANTEX-90 experiment.

The results given in Tables 2.2 and 2.3 point to the primary role of the parameters t_a and Q in forming relationships between the SOA brightness temperatures in the atmospheric water vapor resonance line at 1.35 cm and in the regions (5.4–5.9 mm) of oxygen attenuation (radiation) with the surface heat fluxes.

Table 2.3 Correlation between simulated values of the SOA brightness temperature from various levels of observations at the millimeter and centimeter level and the parameter q_{he} recorded from the vessel *Volna* in April 1990

Wavelength, cm	0.54	0.56	0.59	0.80	1.0	1.35	1.6	3.2	5.0
Satellite	0.48	0.69	0.92	0.87	0.87	0.83	0.88	0.77	0.74
Aircraft	0.77	0.90	0.89	0.84	0.85	0.86	0.88	0.75	0.73
Vessel (1)	0.86	0.87	0.85	0.80	0.81	0.84	0.86	0.74	0.72
Vessel (2)	0.81	0.73	0.71	0.80	0.82	0.78	0.82	0.80	0.70

The cells marked in bold characterize a correlation equal or greater than 0.8

This analysis also shows that independently from the methods of observations used (*satellite, aircraft, or vessel*), the influence of the ocean surface temperature on the SOA brightness temperature is the *passive* factor in comparison with the influence of the atmospheric parameters t_a and Q in the *synoptic* range of time scales.

Figure 2.6 illustrates the important role of the air temperature parameter t_{1500} measured at a height of 1500 m and the atmospheric total water vapor content Q as the transient factor forming the relationship between the SOA brightness temperatures and the near-surface heat fluxes.

We estimated the parameters t_{1500} and Q from aerologic measurements taken aboard vessels during April 8–13, 1990. A close correlation between the vertical turbulent flux of momentum q_v and near-surface wind speed V can be observed. Figure 2.7 demonstrates this effect with data from the ATLANTEX-90 experiment derived from the R/V *Volna*.

This regularity predetermines a clear *direct* correlation between the SOA brightness temperature and the momentum fluxes. For example, we revealed a close

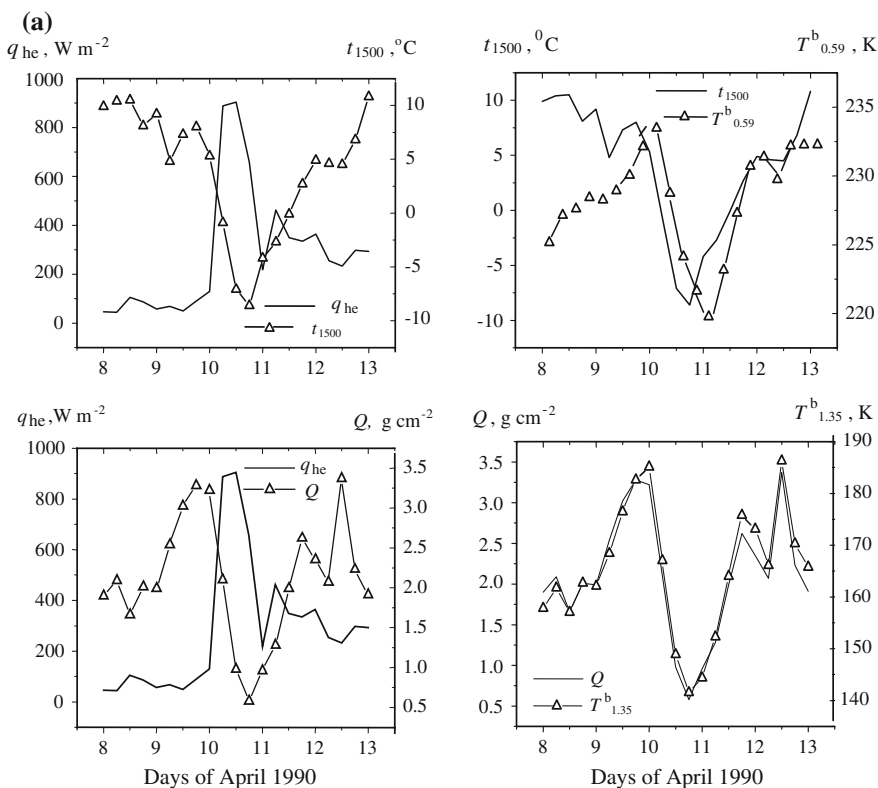


Fig. 2.6 **a** Results of the comparison of heat fluxes q_{he} , atmosphere temperature t_{1500} , total water vapor content of the atmosphere Q , and SOA brightness temperature at the wavelengths of 5.9 mm and 1.35 cm at the point of location of the R/V *Victor Bugaev* during 8–13 April, 1990. **b** The same as (a), but for the vessel *Volna*

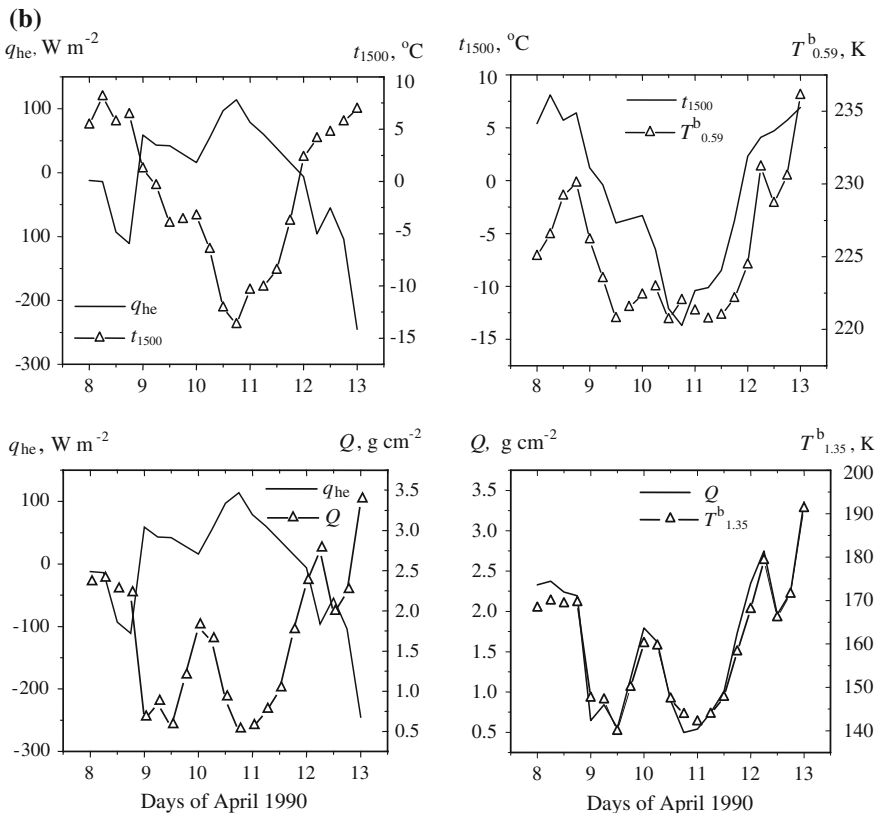


Fig. 2.6 (continued)

interrelationship between momentum fluxes at the ocean–atmosphere interface evaluated from aboard vessels in the ATLANTEX-90 experiment and the model estimates (corresponding to the satellite level of observations) of the SOA brightness temperature in the wavelength range between 3 and 5 cm, which is not affected by the atmosphere; the brightness temperature variations are governed mainly by variations in the intensity of wind stress of the water surface. These results are expected, because, by definition, the momentum flux is connected with wind speed through the air density ρ and drag coefficient C_v (see Formula (1.3) in Chap. 1).

During April 8–13, 1990 the correlation coefficient of variations of the brightness temperature T^b at the wavelength 3.2 cm and the parameter q_v observed from the vessel *Victor Bugaev* was as high as $R = 0.96$ and the discrepancy (rms error) between such variations was $d = 0.043$ for the values of parameter q_v varying from 0.044 to 0.9 N m⁻² (in Newtons per square meter). For the R/V *Musson*, the corresponding parameters were $R = 0.95$ and $d = 0.05$ in the range of variations of q_v 0.013–0.57 N m⁻². Finally, for the vessel *Volna*, the values of its corresponding parameters were $R = 0.89$ and $d = 0.06$ for q_v varying from 0.014 to 0.42 N m⁻².

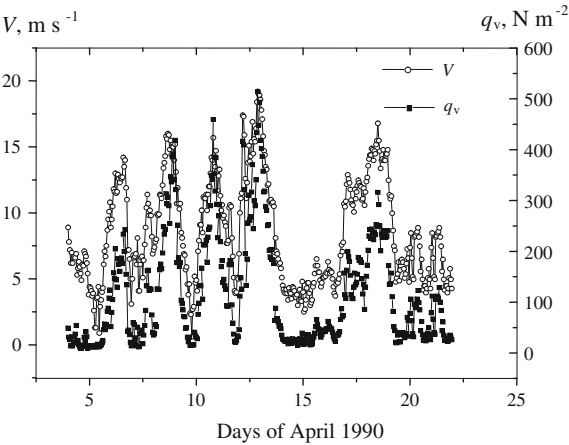


Fig. 2.7 Results of a comparison of the near-surface wind speed and momentum fluxes observed during the stationary phase of the ATLANTEX-90 experiment with a 1-h time resolution for these parameters

2.3.2 Response of the SOA Heat and MCW Radiation Characteristics on Midlatitude Cyclone Passage

Figures 2.2 and 2.3 show that the SOA brightness temperature contrasts in oceanic areas are most pronounced during the passage of cyclones, which result in deep changes of the near-surface air temperature, humidity, and heat fluxes as well as the brightness temperature of the SOA. Evidently, atmospheric enthalpy, which is a direct indicator of horizontal heat and moisture transfer, influences the near-surface heat and integral (averaged over height) MCW radiation characteristics of the system simultaneously and possibly can serve as a transient characteristic between them.

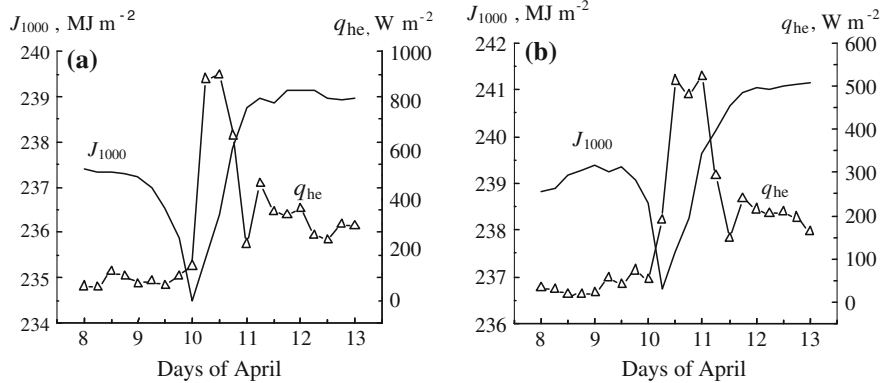


Fig. 2.8 Total heat fluxes q_{he} versus the enthalpy J_{1000} of the ABL during the passage of a cyclone (April 8–13, 1990) through the locations of the (a) Victor Bugaev and (b) Musson

Figure 2.8 compares the values of the atmosphere boundary layer (ABL) enthalpy (computed from aerologic sounding data for horizons at altitudes of 10, 100, 200, 300, 400, 500, 900, and 1000 m gathered aboard the *V. Bugaev* and *Musson* vessels. These values were estimated using the methods stated in Pinus (1982) and Perevedentsev (1984)), with the total heat fluxes excited by the powerful cyclone that originated during the stationary phase of the ATLANTEX-90 experiment on April 8–13, 1990.

Similar results were observed during periods of activity of other midlatitude cyclones in the locations of the R/Vs *V. Bugaev*, *Musson*, and *Volna* during the stationary phase of the ATLANTEX-90 experiment. Therefore, it is possible to consider large-scale horizontal (advective) heat and moisture transfer as a factor that provokes the vertical turbulent fluxes arising for regulating the heat balance between the ocean and atmosphere. A similar effect was marked, for example, by

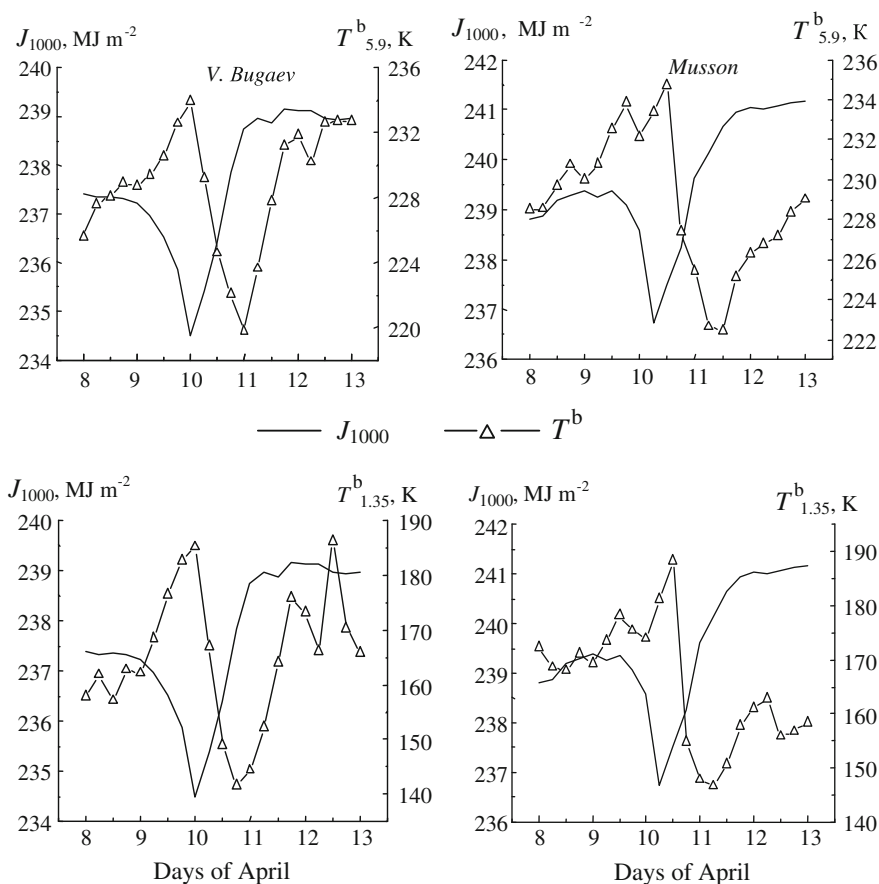


Fig. 2.9 Modeling the response of the SOA brightness temperature at the wavelengths 5.9 mm and 1.35 cm to variations of the ABL enthalpy J_{1000} during the passage of a cyclone (April 8–13, 1990) through the locations of the R/Vs *V. Bugaev* and *Musson*

Abyzyarov et al. (1988), who noted the influence of the so-called zonal circulation index on the boundary heat fluxes in the island region.

Figure 2.9 illustrates the relationships between the ABL enthalpy J_{1000} with SOA brightness temperature variations at the wavelengths 5.9 mm and 1.35 cm over this period.

Figure 2.9 shows that synoptic variations of the enthalpy of the ABL stimulate an appreciable reaction of the SOA brightness temperature in the ranges of the effects of atmospheric oxygen (5–6 mm) and water vapor (1.35 cm), which vary from 12 to 45 K, respectively. Moreover, the response of the brightness temperature lags behind the enthalpy variation by 18–24 h. This property becomes especially apparent during periods of cyclonic activity in the atmosphere, when the ABL temperature and humidity are sharply and strongly varied.

2.4 Conclusions

1. The obtained data show a close correlation between the synoptic variations of the atmospheric temperature and humidity characteristics, as well as the intensity of the ocean–atmosphere heat interaction. The influence of the oceanic surface temperature on the relationships between the SOA brightness temperature and surface heat fluxes is a passive factor in comparison with the near-surface air temperature and humidity.
2. Based on results of the analysis derived in the ATLANTEX-90 experiment, we concluded that variations of the temperature and humidity characteristics in the ABL caused by a large-scale horizontal heat and moisture transfer in the atmosphere *rule* over the vertical turbulent heat and moisture fluxes at the SOA interface, as well as the intensity of natural MCW radiation of the system.
3. The correlation between the SOA brightness temperature and surface heat fluxes is most pronounced for intensive variations in the characteristics of horizontal heat transfer in the atmosphere, particularly for oceanic areas with high cyclonic activity. The brightness temperature of the ocean–atmosphere system in the bands of resonant attenuation of natural MCW radiation in atmospheric water vapor and molecular oxygen appears to serve as the quantitative characteristic of not only the surface sensible and latent fluxes, but also of the atmospheric boundary layer enthalpy in the synoptic range of time scales.

References

- Abuzyarov ZK, Kudryavtseva KI, Seryakov EI, Skriptunova LI (1988) Marine forecasting. Gidrometeoizdat, Leningrad In Russian.
- Basharinov AE, Gurvich AS, Egorov ST (1974) Radio emission of the planet Earth. Nauka, Moscow In Russian.
- Grankov AG, Milshin AA, Soldatov VJu (2010) Computing the response of the ocean-atmosphere system to the heat flux variations. Issledovanie Zemli iz kosmosa 1:55–71 In Russian.
- Gulev SK, Kolinko AV, Lappo SS (1994) Synoptic interaction between the ocean and atmosphere in middle latitudes. Gidrometeoizdat, St. Petersburg In Russian.
- Lappo SS, Gulev SK, Rozhdestvenskii AE (1990) Large-scale heat interaction in the ocean-atmosphere system and energy-active zones in the world ocean. Gidrometeoizdat, Leningrad In Russian.
- Perevedentsev JuP (1984) Circulation and energy processes in the atmosphere. Kazan University, Kazan In Russian.
- Pinus NZ (1982) Available potential energy in the atmosphere and it transformation in the kinetic energy. Meteorologiya i Gidrologiya 4:106-116 In Russian.

Microwave Radiation of the Ocean-Atmosphere

Boundary Heat and Dynamic Interaction

Grankov, A.G.; Milshin, A.A.

2016, XXI, 193 p. 103 illus., 14 illus. in color., Hardcover

ISBN: 978-3-319-21646-1